Mesenchymal Stromal Cells Act as Biopatches for Blood–Retinal Barrier Preservation to Enhance Functional Recovery after Retinal Ischemia/Reperfusion

Xiaoyue Wei, Hanyiqi Mu, Qinmu Zhang, Ziyuan Zhang, Yifei Ru, Kunbei Lai, Yuan Ma, Zhuangling Lin, Rebiya Tuxun, Zitong Chen, Andy Peng Xiang, Tao Li

PII: S2162-2531(24)00332-9

DOI: https://doi.org/10.1016/j.omtn.2024.102445

Reference: OMTN 102445

To appear in: Molecular Therapy: Nucleic Acid

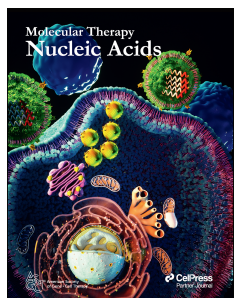
Received Date: 18 June 2024

Accepted Date: 30 December 2024

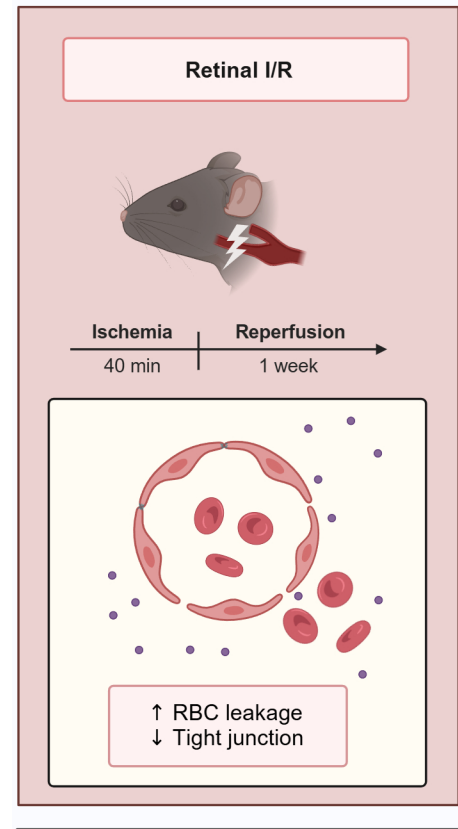
Please cite this article as: Wei X, Mu H, Zhang Q, Zhang Z, Ru Y, Lai K, Ma Y, Lin Z, Tuxun R, Chen Z, Xiang AP, Li T, Mesenchymal Stromal Cells Act as Biopatches for Blood–Retinal Barrier Preservation to Enhance Functional Recovery after Retinal Ischemia/Reperfusion, *Molecular Therapy: Nucleic Acid* (2025), doi: https://doi.org/10.1016/j.omtn.2024.102445.

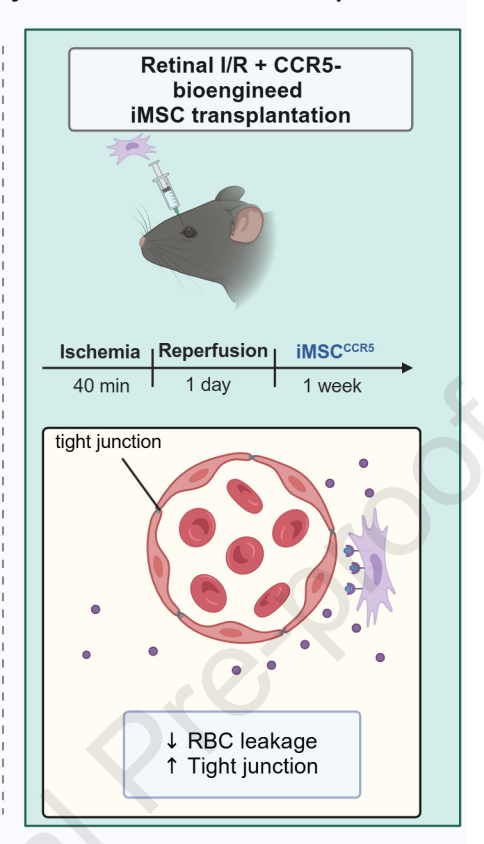
This is a PDF file of an article that has undergone enhancements after acceptance, such as the addition of a cover page and metadata, and formatting for readability, but it is not yet the definitive version of record. This version will undergo additional copyediting, typesetting and review before it is published in its final form, but we are providing this version to give early visibility of the article. Please note that, during the production process, errors may be discovered which could affect the content, and all legal disclaimers that apply to the journal pertain.

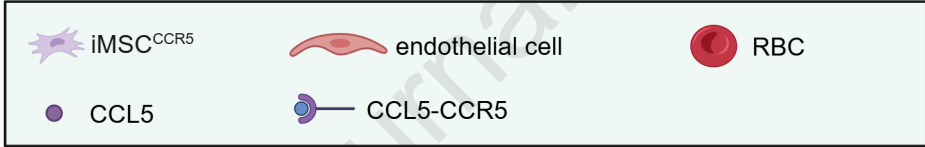
© 2024 Published by Elsevier Inc. on behalf of The American Society of Gene and Cell Therapy.



iMSC^{CCR5} Enhance Functional Recovery After Retinal Ischemia/Reperfusion







- 1 Mesenchymal Stromal Cells Act as Biopatches for Blood-Retinal
- 2 Barrier Preservation to Enhance Functional Recovery after Retinal
- 3 Ischemia/Reperfusion
- 4 Xiaoyue Wei^{1, #}, Hanyiqi Mu^{2, #}, Qinmu Zhang^{2, #}, Ziyuan Zhang², Yifei Ru², Kunbei
- 5 Lai¹, Yuan Ma¹, Zhuangling Lin¹, Rebiya Tuxun¹, Zitong Chen¹, Andy Peng Xiang³, *,
- 6 Tao Li^{1,*}

7

- 8 1. State Key Laboratory of Ophthalmology, Zhongshan Ophthalmic Center, Sun Yat-
- 9 Sen University, Guangzhou, 510230, China;
- 2. Zhongshan School of Medicine, Sun Yat-Sen University, Guangzhou, 510080, China;
- 3. Center for Stem Cell Biology and Tissue Engineering, Key Laboratory for Stem Cells
- and Tissue Engineering, Ministry of Education, Sun Yat-Sen University, Guangzhou,
- 13 510080, China;
- [#] These authors contributed equally to this work.

15

16 *Correspondence

- 17 Professor Andy Peng Xiang, Center for Stem Cell Biology and Tissue Engineering, Sun
- 18 Yat-Sen University, Guangzhou, Guangdong, China. E-mail: xiangp@mail.sysu.edu.cn
- 19 Professor Tao Li, State Key Laboratory of Ophthalmology, Zhongshan Ophthalmic
- 20 Center, Sun Yat-Sen University, Guangzhou, Guangdong, China. E-mail:
- 21 <u>litao2@mail.sysu.edu.cn</u>
- 22 Short title: Gene edited iMSC-based therapy for retinal I/R.

ABSTRACT

23

24

25

26

27

28

29

30

31

32

33

34

35

36

37

38

Retinal ischemia/reperfusion (I/R) is one of the most common pathologies of many vision-threatening diseases and is caused by blood-retinal barrier (BRB) breakdown and the resulting inflammatory infiltration. Targeting BRB is promising for retinal I/R treatment. Mesenchymal stromal cells (MSCs) are emerging as novel therapeutic strategies. Although intravitreal injection targets retina, the restricted number of injected cells still requires the precise biodistribution of MSCs near the injury site. Here, we found that retinal I/R led to BRB breakdown, which induced protein and cell leakage from the circulation. Retinal cell death and diminished visual function were subsequently detected. Moreover, the expression of the chemokine CCL5 increased after retinal I/R, and CCL5 colocalized with the BRB. We then overexpressed CCR5 in human induced pluripotent stem cell-derived MSCs (iMSCs). In vivo, intravitreal injected iMSC^{CCR5} preferentially migrated and directly integrated into the BRB, which preferably restored BRB integrity and eventually promoted retinal function recovery after retinal I/R. In summary, our work suggested that iMSCs act as biopatches for BRB preservation and that iMSC-based therapy is a promising therapeutic approach for retinal diseases related to I/R.

40

INTRODUCTION

41

42

43

44

45

46

47

48

49

50

51

52

53

54

55

56

57

58

59

60

61

62

Retinal ischemia/reperfusion (I/R), a process whereby initial ischemia and subsequent recovery of the blood supply in the retina occur, is one of the most common pathological processes in many vision-threatening diseases, including glaucoma, diabetic retinopathy and central retinal artery occlusion, ^{2,3} and causes 4.68 million cases of blindness per year worldwide.⁴ Current clinical interventions, including pars plana vitrectomy and anti-VEGF injection, target only the middle-to-late stages of retinal I/Rrelated diseases, such as vitreous hemorrhage or neovascularization, when vision loss is likely irreversible.⁵ Pathologically, unlike in peripheral organs, retinal I/R first leads to the disruption of specialized vascular barrier integrity, the blood-retinal barrier (BRB), and then results in inflammatory infiltration, ultimately causing a selfreinforcing destructive cascade involving ganglion cell apoptosis and microglial activation.^{6,7} Hence, an effective way to restore BRB integrity and eventually terminate this microenvironmental cascade at the early stage is promising for clinical transition. Mesenchymal stromal cells (MSCs) represent a promising cell-based therapeutic option for refractory ocular diseases.^{8,9} On the one hand, MSC extracts, including extracellular vesicles (EVs) and microRNAs, alleviate retinal injuries through various biochemical mechanisms. 10,11 The administration of MSC-derived EVs (MSC-EVs) in a glaucoma model enhances retinal function recovery by decreasing neuroinflammation and apoptosis in retinal tissue.¹¹ MicroRNA192 from MSC-EVs relieves the inflammatory response and angiogenesis in oxygen-induced retinopathy. ¹⁰ On the other hand, MSCs provide structural support for specialized structures that MSC extracts do 63

64

65

66

67

68

69

70

71

72

73

74

75

76

77

78

79

80

81

82

83

84

not preform. MSCs improve fracture healing by directly targeting the injury site and functioning as bioscaffolds for osteogenesis. 12,13 Additionally, for barrier preservation, MSCs contribute to the vasoconstriction capacity of the blood-brain barrier (BBB), mimicking an in vitro model. 14 Thus, we speculated that MSCs could patch the BRB by providing structural support in retinal I/R in vivo. However, primary MSCs have limited passages in vitro and exhibit biological and functional heterogeneity, which may raise concerns about their safety and effectiveness.¹⁵ Previous study in our lab has generated highly homogeneous MSCs derived from human induced pluripotent stem cells (hiPSCs), which showed considerable similarity in function.¹⁶ Moreover, since hiPSCs can differentiate into homogeneous MSCs in a large quantity, ¹⁷ hiPSC-derived MSCs (iMSCs) can be a homogenous and unlimited source for cell therapy in future clinical applications. ¹⁸ Other obstacles limiting the clinical application of MSCs include their unsatisfactory homing and planting capacity. 19,20 For retinal disease treatment, although intravitreal injection targets the retina, the restricted number of injected cells still requires the precise biodistribution of MSCs near the injury site. 21,22 Chemokine ligands and chemokine receptors guide the directional trafficking of MSCs not only for organ-specific migration but also for niche-specific distribution within organs. MSCs can help repair diabetic skin wounds, where they transdifferentiate into multiple skin cell types to assist regenerative wound healing via the CXCL16-CXCR6 axis.²³ Additionally, the CXCL12-CCR4 axis plays an important role in the homing of MSCs to the hematopoiesis niche in the bone marrow, ^{24,25} while the CCL3-CCR1 axis is involved in MSC migration to bone fracture sites for

osteogenesis.²⁶ Therefore, we hypothesized that genetically edited iMSCs that express the proper chemokine receptor would migrate to the BRB, improve BRB integrity and eventually promote retinal function recovery after retinal I/R.

88

89

90

91

92

93

94

95

96

97

98

99

100

101

102

103

104

105

106

85

86

87

RESULTS

Blood-retinal barrier disruption after retinal I/R

To investigate the impact of I/R on retinal tissue, we first established a retinal I/R model through internal carotid artery occlusion (ICAO) (Fig. S1A) and employed immunofluorescence staining to assess the integrity of the BRB at 6 hours (6 h), 1 day (1 d) and 3 days (3 d) after retinal I/R, which can be reflected by tight junction coverage and pericyte coverage. 27,28 The integrity of Claudin5, a tight junction protein, and pericyte coverage were compromised after retinal I/R and deteriorated over time (Fig. 1A-D). The integrity of ZO-1, another tight junction protein of the BRB, also decreased at 1 d after retinal I/R (Fig. S1B, D). For further verification, we focused on the leakage of serum protein and red blood cells (RBCs) in retinal tissue. Immunofluorescence staining revealed serum protein fibrinogen leakage and RBC leakage into retinal tissue after retinal I/R, which increased over time (Fig. 1E-H). Additionally, F4/80⁺ macrophages emigrated from blood vessels and infiltrated retinal tissue after retinal I/R (Fig. S1C, E). Taken together, these results confirmed that retinal I/R resulted in breakdown of the BRB, which deteriorated over time. Since the resulting inflammatory infiltration is an essential driver of the destructive retinal I/R cascade, 29 retinal cell death was determined via in situ terminal deoxynucleotidyl transferase dUTP nick end

labeling (TUNEL) staining. For completeness of inquiry and clarity of expression, we artificially divided the retina into three different positions according to the anatomy, including the center (within 200 µm of the optic disc), far-periphery (retinal margin), and mid-periphery (between the 2 positions stipulated above). Retinal section staining revealed that the degree of apoptosis at each position increased with time after retinal I/R (Fig. 1I, J).

113

114

115

116

117

118

119

120

121

122

123

124

125

126

127

128

107

108

109

110

111

112

The expression of CCL5 increased after retinal I/R

There are multiple mechanisms underlying I/R injury, including calcium overload, oxidative stress and mitochondrial dysfunction. 30,31 Retinas from the sham and I/R groups were obtained 1 d after retinal I/R for transcriptome sequencing to investigate changes in the retinal microenvironment and outstanding pathways after retinal I/R and identify potential therapeutic targets. Kyoto Encyclopedia of Genes and Genomes (KEGG) analysis suggested that the interaction of chemokines and corresponding receptors might play an important role (Fig. 2A), and the spectrum of chemokines changed greatly after retinal I/R (Fig. S2A). Considering that the chemokine/chemokine receptor axis is indispensable for MSC migration, we next obtained retinas 1 d after retinal I/R to detect the mRNA levels of chemokines, which were reported to be associated with I/R changes, 32,33 including CCL2, CCL5, CCL7, CCL12, CXCL2, and CXCL12, and found that the mRNA level of *Ccl5* increased most markedly (Fig. 2B). Furthermore, the mRNA level of Ccl5 peaked at 1 d after retinal I/R (Fig. 2C), suggesting the potential optimal therapeutic timing. Moreover, flow cytometry analysis

revealed that the expression of CCL5 in retinas increased at 1 d after retinal I/R (Fig. 2D, E). Since retinal I/R leads to BRB damage, we next explored the relationship between CCL5 and the BRB. Immunofluorescence staining revealed that more than 50% of the vessels colocalized with CCL5 in the superficial, intermediate and deep layers (Fig. 2F, G; Fig. S3A), which suggested that retinal vessels could be targeted via the CCL5–CCR5 axis. In addition, Gene set enrichment analysis (GSEA) revealed microenvironmental changes, including immune activation, matrix and vasculature reorganization and neuronal system degeneration in the retina after retinal I/R (Fig. S4A-C). Together, these results presented that the expression of CCL5 increased and peaked at 1 d after retinal I/R in the retina and CCL5 prominently colocalized with the BRB, suggesting that targeting the BRB via chemotaxis of CCL5 at 1 d after retinal I/R could be promising.

Overexpression of CCR5 improved the migratory capacity of iMSCs in response

to CCL5

MSC-based therapy may serve as a potential intervention for retinal I/R-related diseases. To eliminate the heterogeneity of MSCs, we differentiated hiPSCs, which expressed stemness markers, including Nanog, Oct4, and Sox2 (Fig. S5B), into MSCs according to methods reported previously (Fig. S5A). MSCs still had adipogenic, osteogenic, and chondrogenic potential (Fig. S5C) and exhibited a typical MSC surface pattern, in which CD29, CD44, CD73 and CD90 were positive and CD34 and CD45 were negative (Fig. S5D). Next, in light of increased CCL5 colocalized with the BRB

151	after retinal I/R, we speculated that iMSCs could be recruited to the damaged BRB via
152	the CCL5-CCR5 axis, which may improve the effect of MSC-based therapy.
153	Considering that MSCs express chemokine receptors at an almost negligible level, ³⁴ we
154	transduced iMSCs with lentiviral vectors encoding CCR5 (referred to as iMSC ^{CCR5}) or
155	tdTomato (referred to as iMSCtdTomato) to increase CCR5 expression. The cells
156	expressing tdTomato fluorescence were isolated via flow cytometry, and the mRNA and
157	protein levels of CCR5 were determined (Fig. S5E-G).
158	We next focused on the migratory capacity of iMSC ^{CCR5} in response to CCL5. First,
159	we compared the migratory capacity of iMSCCCR5 and iMSCtdTomato under the
160	recruitment of human CCL5 (hCCL5) and murine CCL5 (mCCL5) respectively. In vitro
161	transwell migration assays revealed that iMSC ^{CCR5} had greater migratory capacity than
162	iMSC ^{tdTomato} in both the hCCL5 and mCCL5 groups, and human iMSC ^{CCR5} also
163	responded to mCCL5 (Fig. 3A, B). Next, we explored whether iMSC ^{CCR5} also had
164	greater migratory and planting capacity in vivo. One day after retinal I/R, the mice from
165	the I/R groups and sham groups both received intravitreal injections of iMSC ^{tdTomato} or
166	iMSC ^{CCR5} . Then, the mice were sacrificed at 4 days post-transplantation (4 dpt) and 7
167	days post-transplantation (7 dpt), and the number and biodistribution of iMSCs in the
168	retina were detected and quantified. Compared with iMSCtdTomato, iMSCCCR5
169	preferentially migrated and integrated into the BRB at both 4 dpt and 7 dpt in the I/R
170	groups but not in the sham groups (Fig. 3C, D). Overall, we successfully established a
171	homogeneous iMSC lineage and overexpressed CCR5 in iMSCs. Additionally, we
172	demonstrated that iMSC ^{CCR5} exhibited increased migratory capacity in vitro and was

preferably integrated into the BRB as a biopatch *in vivo*.

174

175

176

177

178

179

180

181

182

183

184

185

186

187

188

189

190

191

192

193

194

iMSC^{CCR5} infusion protected against damage to the BRB and visual function

caused by retinal I/R

Since iMSC^{CCR5} migrated and integrated to blood vessels, we focused on whether iMSC^{CCR5} could effectively restore BRB integrity as well as retinal function after retinal I/R. For this purpose, mice received intravitreal injections of PBS, iMSC^{tdTomato} or iMSC^{CCR5} at 1 d after retinal I/R, and retinas were obtained at 7 d after iMSC injection for further investigation (Fig. 4A). First, we employed immunofluorescence staining to detect the integrity of the BRB. Compared with the PBS and iMSC^{tdTomato} groups, the iMSC^{CCR5} group presented less attenuation of Claudin5 coverage and pericyte coverage and less leakage of RBCs and fibrinogen, suggesting that iMSC^{CCR5} effectively restored BRB integrity (Fig. 4B-D, F; Fig. S6A, B). In addition, TUNEL staining revealed decreased degree of apoptosis in each position of the retina (Fig. 4E). Furthermore, iMSC^{CCR5} treatment effectively increased the amplitudes of a- and b-waves and decreased implicit times compared with those in the PBS and iMSCtdTomato treatment, suggesting retinal function recovery, as shown by ERG (Fig. 5A, B). Besides, we also focused on the long-term effect of iMSC^{CCR5} treatment on retinal function recovery. ERG was analyzed 2 months after iMSC^{CCR5} injection, and the results showed that iMSC^{CCR5} treatment enhanced retinal function recovery compared with PBS and iMSC^{tdTomato} treatment in a long term (Fig. S7A, B). Taken together, these findings suggested that intravitreal injection of iMSC^{CCR5} could protect against BRB damage

and enhance retinal function recovery following retinal I/R.

In conclusion, we revealed BRB breakdown following retinal I/R and the resulting vascular content leakage, eventually leading to retinal cell death. Next, we found that the chemokine-chemokine receptor pathway was significantly involved in retinal I/R-related changes and that CCL5 expression increased most markedly and strongly colocalized with the BRB. Then, we generated the iMSC^{CCR5} lineage, which exhibited better migratory capacity *in vitro*. *In vivo*, iMSC^{CCR5}, acting as "biopatches", could enhance BRB integrity via direct integration into the BRB, thus improving retinal function recovery after retinal I/R (Fig. 6).

DISCUSSION

In the present study, retinal I/R led to BRB breakdown and vascular content leakage, resulting in retinal cell death and deterioration of visual function. Additionally, we examined the changes in the spectrum of chemokines following retinal I/R and found that CCL5 expression increased most markedly and remarkably around retinal vessels. Given the importance of the chemokine/chemokine receptor axis in cell migration, we engineered iMSC^{CCR5}, which displayed enhanced migratory capacity *in vitro*. *In vivo*, infused iMSC^{CCR5} preferentially migrated and directly integrated into the BRB, which notably patched the BRB and improved the retinal function recovery after retinal I/R.

Given their tissue regeneration capacity and safety, MSCs have become potential candidates for cell therapy and translational medicine. The application of MSC-based therapy is promising for treating I/R in both peripheral organs and the central nervous

system (CNS) through multiple mechanisms. ³⁵ In peripheral organs, exogenous MSCs
mainly protect parenchymal cells directly against I/R injury through their anti-apoptotic
anti-inflammatory or antioxidative effects. For example, MSC-derived microRNA had
cardioprotective effects against myocardial I/R injury by improving inflammation and
pyroptosis in myocardial cells. ³⁶ Additionally, MSCs had anti-apoptotic effect on
alveolar epithelial cells and ameliorated I/R injury after lung transplantation. ³⁷
Furthermore, in renal I/R, MSC-EVs protected tubular epithelial cells against oxidative
insult.38 On the other hand, unlike peripheral organs, CNS homeostasis maintenance
requires specialized vascular barrier integrity, which is indispensable for immune
privilege and a defined microenvironment of the CNS. Given the importance of the
CNS barrier, it is believed that MSCs not only protect against neuronal apoptosis but
also restore the integrity of the BBB to avoid downstream damage after ischemic
stroke. ³⁹ Similarly, in our study, we also reported that iMSCs restored the integrity of
the BRB and alleviated the apoptosis of retinal neural cells after retinal I/R. Based on
special structure and function of these barriers discussed above and our findings,
protection and repair of these barriers constitute unique therapeutic mechanisms of
MSC-based therapy for I/R injury to the CNS.
The BBB and BRB, as blood-neural barriers, have a similar structure and play an
important role in reliable neuronal activity by maintaining a precisely adjustable
microenvironment.40 The BBB is the bridge between blood and brain tissue and is
composed mainly of brain capillary endothelial cells, base membrane, glial membrane
and peripheral pericytes and astrocytes. These specifically and finely developed

structures allow the BBB to mechanically prevent substances such as toxins, drugs and
pathogens from entering the brain. In addition, due to the existence of different types
of transporters on endothelial cells, nutrients and metabolites can smoothly pass
through to maintain the homeostasis of the microenvironment of the nervous system.
The intact BBB structure and functions are essential for structural and functional brain
connectivity, synaptic activity and information processing. ⁴¹ Similarly, the BRB is a
typical neurovascular unit that is characteristic of the retina. ⁴² Suggested to be
composed of tightly conjunct endothelial cells combined with pericytes, astrocytes,
microcytes and Müller cells, the BRB shares an analogous mechanism with the BBB in
that it excludes immune cells and prevents disturbing substances from entering retinal
tissue. ⁴³ Breakdown of the BBB or BRB, induced by pathologically increased levels of
vascular endothelial growth factor or other mediators in the occurrence of pathological
conditions such as trauma, I/R or tumor, can result in vasogenic edema and significant
clinical problems such as brain morbidity or vision loss, respectively. ⁴⁴
MSC-based therapy for CNS barrier preservation is promising. For BBB
preservation, MSCs are mainly given by intravenous injection. As most intravenously
infused MSCs are distributed in the lungs, pulmonary microembolism is considered as
an adverse effect. ⁴⁵ Although MSCs are capable of transendothelial migration to
infiltrate the brain, reaching enough cells for treatment is difficult. ⁴⁶ Therefore, for
safety and efficacy considerations, the intravenous injection of MSC-EVs is superior to
the intravenous injection of MSCs for BBB treatment because of their small diameter

Notch1 signaling in endothelial cells, upregulating VEGF receptor 1 expression in
pericytes, ⁴⁷ or inhibiting nuclear transcription factor-kappaB signaling in astrocytes. ⁴⁸
The above limitations of MSCs could be avoided by intravitreal injection for BRB
preservation. In addition to repairing barriers through biochemical mechanisms similar
to those of MSC-EVs, the structural support capacity of MSCs is advantageous over
that of MSC-EVs. 45 In our study, we found that iMSCs can directly integrate into the
BRB and act as biopatches for BRB preservation. Our results showed that iMSCs are
promising future therapeutic candidates for treating retinal I/R-related diseases.

MATERIALS AND METHODS

Ethics statement

All animal experiments in this study complied with the guidelines of Sun Yat-sen University and were approved by the Ethics Committee of Sun Yat-sen University (2021001559, 2024000008).

Animals and retinal I/R model

Male WT C57BL/6 mice (8–10 weeks old) were purchased from Guangdong Medical Laboratory Animal Centre (Guangzhou, China). All mice were provided free access to a standard rodent diet and drinking water and were kept in a colony room with a 12-h light/12-h dark cycle at the Sun Yat-sen University Animal Centre. The internal carotid artery (ICA) provides blood to the retina through the ophthalmic artery;⁴⁹ thus, the retinal I/R model was generated as follows: the mice were anesthetized with 1.5%

isoflurane in a 30% $O_2/69\%$ N_2O mixture, and a heating pad was used to maintain the body temperature at 37 ± 0.5 °C. Unilateral ligation (left side) of the ICA was performed using a 6/0 surgical suture for 40 minutes of ischemia, after which the suture was removed to allow reperfusion for 6 hours, 1 day or 3 days.

287

288

289

290

291

292

293

294

295

296

297

298

299

300

301

302

303

283

284

285

286

Generation and identification of iMSCs

To differentiate hiPSCs into MSCs, the procedure was performed as previously described. 16 First, hiPSCs established as described were differentiated into neuromesodermal progenitors (NMPs). 50 Confluent hiPSCs were isolated into single cells by incubation with Accutase for 2-3 minutes at 37 °C. Single cells were subsequently seeded into Matrigel-coated plates and cultured for 24 hours in mTeSR medium supplemented with 10 µM Y27632 (Sigma-Aldrich, St. Louis, MO, USA). For NMP differentiation, these cells were then cultured in Essential 6 medium containing 20 ng/ml basic fibroblast growth factor (bFGF), with or without 2–5 ng/ml transforming growth factor-\(\beta\)1 (TGF\(\beta\)1) (both from Pepro Tech, Rocky Hill, NJ, USA), and 10 \(\mu\)M Chir99021 (Stemgent, Cambridge, MA, USA) for 2-5 days. For MSC differentiation, paraxial mesoderm cells that had been differentiated in medium supplemented with bFGF, TGFβ1, and Chir99021 for 4-5 days were subsequently cultured in MesenCultTM-ACF Plus Medium (Stemcell Technologies, Vancouver, Canada) for 2–3 weeks. The typical markers of MSCs were identified through flow cytometry as described below.

Cell culture

iMSCs were cultured in MesenCultTM-ACF Plus Medium supplemented with 10% fetal bovine serum (FBS) and 1% penicillin and streptomycin and were incubated in 5% CO₂ at 37 °C.

Multiple differentiation potential of iMSCs

Multiple differentiation assays, including osteogenic induction, adipogenic induction, and chondrogenic induction, were performed as previously described. ^{51,52} For osteogenic induction, iMSCs were cultured in alpha MEM medium supplemented with 100 nM dexamethasone, 10 mM β -glycerophosphate, 50 mM ascorbic acid-2-phosphate (Sigma–Aldrich, St. Louis, MO, USA), 10% FBS and 1% penicillin and streptomycin for 21 days. Then, the osteoblasts were fixed in cold 95% ethanol for 5 minutes and stained with 2% Alizarin Red solution.

For adipogenic induction, iMSCs were cultured in alpha MEM medium supplemented with 1 mM dexamethasone, 500 mM 3-isobutyl-1-methylxanthine, 10 mg/mL insulin, 100 mM indomethacin (Sigma–Aldrich, St. Louis, MO, USA), 10% FBS, and 1% penicillin and streptomycin for 21 days. Subsequently, the resulting cells were fixed with 4% paraformaldehyde (PFA; Phygene, Fuzhou, China) for 30 minutes at room temperature and stained with fresh Oil Red O solution for 50 minutes.

For chondrogenic induction, the cells were cultured in a 15-ml conical tube containing differentiation basal medium (Sigma-Aldrich, St. Louis, MO, USA), which was changed every 3 days. After 21 days, the cell clumps were fixed in 4% PFA and

stained with toluidine blue.

Intravitreal injection

Intravitreal injection was performed under a stereomicroscope as previously described. The mice were anesthetized as described above, and then the eyes were prepped with topical anesthetic. A cell suspension containing $1\times10^4\,\mathrm{iMSCs}$ in $0.5\,\mu\mathrm{L}$ of PBS was slowly injected into the vitreous cavity of model eyes via a microinjector (Hamilton, Shanghai, China). The same volume of PBS was injected into the eyes of the control group.

Retina processing and immunofluorescence

The mice were anesthetized as described above and perfused with ice-cold saline followed by 4% PFA. For immunofluorescence of whole-mounted neural retinas, eyeballs were removed and fixed in 4% PFA for 15 minutes at 4 °C. After the cornea and crystalline lens were removed, the residual part was fixed in 4% PFA for 3 hours at 4 °C. The retinas were removed by orbital dissection, washed with PBS, and permeabilized in PBS containing 5% BSA (Phygene, Fuzhou, China) and 0.5% Triton X-100 (Sangon Biotech, Shanghai, China) overnight at 4 °C. For immunofluorescence of retinal sections, eyeballs were removed, fixed in 4% PFA overnight at 4 °C, and cut into 20 µm frozen cryosections. Retinal sections were fixed in 4% PFA for 20 minutes, permeabilized in 0.15% Triton X-100 for 15 minutes, and blocked with PBS-5% normal goat serum (BOSTER, Pleasanton, CA, USA) for 1 hour. Both whole-mounted neural

retinas and retinal sections were incubated with appropriate primary and secondary antibodies. Images were captured using Dragonfly high-speed confocal microscopy (ANDOR, Oxford Instruments, Oxford, UK). For immunofluorescence of cells, the hiPSCs were fixed with 4% PFA at room temperature for 20 minutes and rinsed three times with PBS. Then, the cells were permeabilized with 0.3% Triton X-100 in PBS and incubated overnight at 4 °C with primary antibodies. Secondary antibodies were incubated for 2 hours at room temperature. The samples were counterstained with 4',6-diamidino-2-phenylindole (DAPI; Sigma–Aldrich, St. Louis, MO, USA). Images were captured using a confocal laser-scanning microscope (LSM 880; Carl Zeiss, Jena, Germany). All of the utilized antibodies are listed in Supplemental Table 1.

TUNEL staining

The number of apoptotic cells in neural retinas was determined via TUNEL staining using a TUNEL Apoptosis Assay Kit (Thermo Fisher Scientific, Waltham, MA, USA), and the nuclei were stained with DAPI. Images were captured using Dragonfly high-speed confocal microscopy.

Isolation of retinal and cellular RNA and quantitative real-time polymerase chain reaction (qRT-PCR)

The mice were directly sacrificed by an overdose of sodium pentobarbital without perfusion, after which the retinas were removed and dissociated. For iMSCs, cell pellets were collected. Total RNA was extracted from retinas or iMSCs using a RNeasy mini

kit (QIAGEN, Duesseldorf, Germany) according to the manufacturer's instructions,
and RNA quality control was performed using a Nanodrop 2000 (Thermo Fisher
Scientific, Waltham, MA, USA). Then, cDNA was reverse transcribed using a Revert-
Aid First Strand cDNA Synthesis Kit (Thermo Fisher Scientific, Waltham, MA, USA).
SYBR Green qRT-PCR Super Mix (Roche, Basel, Switzerland) was used to conduct
RT-PCR, which was performed using a Light Cycler 480 detection system (Roche,
Basel, Switzerland) as previously described. ⁵⁴ The sequences of primers used in this
study are presented in Supplemental Table 4.

Flow cytometric analysis of retinas and iMSCs

The mice were anesthetized as described above and perfused with ice-cold saline followed by 4% PFA, and the retinas were isolated. The retinas were mechanically homogenized and passed through 40 µm filters. For iMSCs, the cells were trypsinized and collected. After centrifugation, the cell pellets were resuspended and washed 3 times with PBS. Both the retinal cell suspension and the iMSCs were stained with the appropriate antibodies listed in Supplemental Table 2. Fluorescence-activated cell sorting (FACS) was performed using CytoFLEX and CytoFLEX s (Beckman Coulter, CA, USA) flow cytometers.

Western blotting

The cells were extracted and sonicated in RIPA buffer (Beyotime, Shanghai, China) containing protease and phosphatase inhibitors (Roche, Basel, Switzerland), and the

resulting supernatant was centrifuged. The protein concentration was then measured using a BCA protein assay kit (Cwbiotech, Beijing, China) and normalized across samples. Equal amounts of protein were resolved and separated by SDS-PAGE and then electrotransferred onto a 0.45-µm-pore size polyvinylidene difluoride membrane (Millipore, Boston, MA, USA). The membranes were blocked with 5% nonfat milk (Phygene, Fuzhou, China) for 1 hour and then incubated with the appropriate primary antibodies overnight at 4 °C. Specifically, bound primary antibodies were detected using horseradish peroxidase-coupled secondary antibodies and enhanced chemiluminescence (Millipore, Boston, MA, USA). The primary and secondary antibodies are listed in Supplemental Table 3.

Vector construction and lentiviral transduction

To generate iMSC^{tdTomato} and iMSC^{CCR5} lines, lentiviruses containing the tdTomato vector and CCR5-overexpressing vector respectively were purchased from WZ biosciences Company (Shandong, China). Before lentiviral transduction, iMSCs were seeded into 24-well plates and incubated in 5% CO₂ at 37 °C overnight. The optimal cell density for lentiviral transduction is approximately 50%. The medium was subsequently removed, and 2 ml of fresh complete medium supplemented with 6 μg/ml polybrene was added. The lentiviruses were added to the cells at an MOI of 10. Twenty-four hours later, the medium containing the lentiviruses was replaced with fresh medium. At 48 to 72 hours after lentiviral transduction, the expression of red fluorescence protein (RFP) was observed via fluorescence microscopy to determine the

transfection efficiency. Then, the RFP⁺ iMSCs were sorted through FACS and used for subsequent experiments. Quantitative PCR and western blotting were performed to detect the CCR5 mRNA and protein levels, respectively, in the iMSC^{CCR5} line.

Transwell migration assay

Transwell migration assays were performed using transwell chambers (24-well plate, 8-μm pore size; Corning Incorporated, Corning, NY, USA). iMSC^{CCR5} or iMSC^{tdTomato} were suspended in serum-free medium and adjusted to a density of 1 × 10⁵ cells/ml. One hundred microliters of cell suspension was added to the upper chamber of the migration well. In contrast, 100 μL of serum-free medium supplemented with the chemokine mCCL5 (100 ng/ml) or hCCL5 (50 ng/ml) (MedChem Express, Monmouth Junction, NJ, USA) was loaded into the lower chamber. Twenty-four hours later, the cells that migrated through the underside of the insert membrane were fixed with 4% PFA for 30 minutes and stained with crystal violet (Beyotime, Shanghai, China) for 20 minutes. Then, the cells in five random separate microscope fields were counted (400x magnification).

Electroretinography

To evaluate the visual function of the mice, photopic flash electroretinography (ERG) was performed using Diagnosys Espion system (Diagnosys LLC, Lowell, MA, USA). To demonstrate the effect of iMSC treatment, ERG was performed at 1 week after intravitreal injection. Before the ERG test, the mice were incubated in a dark

environment for 12 hours and then anesthetized as described above, after which the
pupils were dilated with 0.5% tropicamide (Macklin, Shanghai, China). Ring-shaped
gold recording electrodes were placed on the cornea of both eyes. A pair of reference
needle electrodes made of stainless steel were placed subcutaneously behind the ears,
and a ground electrode was placed subcutaneously by the tail. After 10 minutes of
adaptation to green light at 5 cd.s/m ² , the eyes of the tested mouse were exposed to a
series of light flashes ranging from 0.01 to 3 cd.s/m ² , with 32 flashes at each light
intensity and 0.5 seconds as the interval of each flash. The body temperature of the mice
was maintained at 37 \pm 0.5 $^{\circ}\text{C}$ with a heating pad throughout the entire procedure. The
results were analyzed for a-wave, b-wave, and implicit time using ERGView 4.380R
software (OcuScience, Henderson, NV, USA).

KEGG pathway analysis

Transcriptome sequencing was performed by Suzhou PANOMIX Biomedical Tech Co., Ltd. KEGG pathway enrichment analysis was performed via the Bioconductor package "GeneAnswers" to identify critical pathways closely related to the impact of I/R on the retina. P < 0.05 was considered to indicate statistical significance and to achieve significant enrichment.

GSEA

457	GSEA was conducted, and the plots were generated at http://www.webgestalt.org/.
458	All P values were corrected for multiple testing methods, and the thresholds for
459	significant enrichment were $P < 0.05$ and FDR < 0.25 .
460	
461	Scheme creation
462	All the schemes used in this study were created with BioRender (BioRender
463	Toronto, Canada; https://www.biorender.com/).
464	
465	Statistical analysis
466	GraphPad Prism 8 software (San Diego, CA, USA) was used for all the statistical
467	analyses. ImageJ 1.52a software (Wayne Rasband, MD, USA) was used to analyze the
468	immunostaining images. CytExpert 2.0 software (Beckman Coulter, CA, USA) and
469	FlowJo V.10.0 software (Mario Roederer, OR, USA) were used to analyze the FACS
470	data. Ingenuity Pathway Analysis (IPA; Version: 52912811) software (Ingenuity
471	Systems, Inc.) was used to analyze the RNA-Seq data. The data obtained from multiple
472	experiments were presented as the mean \pm SEM. Depending on the data, Student's t
473	test and one-way and two-way analysis of variance (ANOVA) were used for
474	comparisons and indicated in the legends of each figure. Differences were considered
475	significant when $P < 0.05$.

AVAILABILITY OF DATA AND MATERIALS

478	The data that support the findings of this study are available from the corresponding
479	author upon reasonable request.
480	
481	ACKNOWLEDGEMENTS
482	We would like to thank other members from the State Key Laboratory of
483	Ophthalmology, Sun Yat-Sen University, and the Center of Stem Cells and Tissue
484	Engineering, Sun Yat-Sen University, for their help and suggestions. The graphical
485	abstract was created using BioRender.
486	
487	AUTHOR CONTRIBUTIONS
488	X.W., H.M., and Q.Z. designed and performed the experiments. Z.Z. and Y.R.
489	analyzed the data and wrote the manuscript. K.L., Y.M. and Z.L. performed the
490	statistical analysis. R.T. and Z.C. conducted the investigation. AP.X. and T.L.
491	supervised the study. All the authors read and approved the final manuscript.
492	
493	DECLARATION OF INTERESTS
494	The authors declare that they have no competing interests.
495	
496	KEYWORDS
497	Mesenchymal stromal cells, Cell therapy, Retinal ischemia/reperfusion, Blood-retinal
498	barrier
499	

REFERENCES

- Lu, C., Wang, C., Xiao, H., Chen, M., Yang, Z., Liang, Z., Wang, H., Liu, Y., Yang, Y., and
- Wang, Q. (2021). Ethyl pyruvate: A newly discovered compound against ischemia-
- 503 reperfusion injury in multiple organs. Pharmacol Res *171*, 105757. 504 10.1016/j.phrs.2021.105757.
- 505 2. Bresnick, G.H., De Venecia, G., Myers, F.L., Harris, J.A., and Davis, M.D. (1975). Retinal 506 ischemia in diabetic retinopathy. Arch Ophthalmol *93*, 1300-1310. 507 10.1001/archopht.1975.01010020934002.
- Tang, L.H.C., Fung, F.K.C., Lai, A.K.W., Wong, I.Y.H., Shih, K.C., and Lo, A.C.Y. (2021).

 Autophagic Upregulation Is Cytoprotective in Ischemia/Reperfusion-Injured Retina and
- Retinal Progenitor Cells. Int J Mol Sci 22. 10.3390/ijms22168446.
- 511 4. Burton, M.J., Ramke, J., Marques, A.P., Bourne, R.R.A., Congdon, N., Jones, I., Ah Tong,
- B.A.M., Arunga, S., Bachani, D., Bascaran, C., et al. (2021). The Lancet Global Health
- Commission on Global Eye Health: vision beyond 2020. Lancet Glob Health 9, e489-e551.
- 514 10.1016/s2214-109x(20)30488-5.
- 515 5. Tan, G.S., Chakravarthy, U., and Wong, T.Y. (2020). Anti-VEGF Therapy or Vitrectomy
- Surgery for Vitreous Hemorrhage From Proliferative Diabetic Retinopathy. Jama *324*,
- 517 2375-2377. 10.1001/jama.2020.22829.
- 518 6. Minhas, G., Sharma, J., and Khan, N. (2016). Cellular Stress Response and Immune
- Signaling in Retinal Ischemia-Reperfusion Injury. Front Immunol 7, 444.
- 520 10.3389/fimmu.2016.00444.
- 521 7. Osborne, N.N., Casson, R.J., Wood, J.P., Chidlow, G., Graham, M., and Melena, J. (2004).
- Retinal ischemia: mechanisms of damage and potential therapeutic strategies. Prog Retin
- 523 Eye Res *23*, 91-147. 10.1016/j.preteyeres.2003.12.001.
- 524 8. Uccelli, A., Moretta, L., and Pistoia, V. (2008). Mesenchymal stem cells in health and disease.
- 525 Nat Rev Immunol *8*, 726-736. 10.1038/nri2395.
- 526 9. Oh, J.Y., and Lee, R.H. (2021). Mesenchymal stromal cells for the treatment of ocular
- autoimmune diseases. Prog Retin Eye Res *85*, 100967. 10.1016/j.preteyeres.2021.100967.
- 528 10. Gu, C., Zhang, H., and Gao, Y. (2021). Adipose mesenchymal stem cells-secreted
- extracellular vesicles containing microRNA-192 delays diabetic retinopathy by targeting
- 530 ITGA1. J Cell Physiol *236*, 5036-5051. 10.1002/jcp.30213.
- 531 11. Mathew, B., Ravindran, S., Liu, X., Torres, L., Chennakesavalu, M., Huang, C.-C., Feng, L.,
- Zelka, R., Lopez, J., Sharma, M., et al. (2019). Mesenchymal stem cell-derived extracellular
- vesicles and retinal ischemia-reperfusion. Biomaterials 197, 146-160.
- 534 10.1016/j.biomaterials.2019.01.016.
- 535 12. Méndez-Ferrer, S., Michurina, T.V., Ferraro, F., Mazloom, A.R., Macarthur, B.D., Lira, S.A.,
- Scadden, D.T., Ma'ayan, A., Enikolopov, G.N., and Frenette, P.S. (2010). Mesenchymal and
- haematopoietic stem cells form a unique bone marrow niche. Nature 466, 829-834.
- 538 10.1038/nature09262.
- 539 13. Park, D., Spencer, J.A., Koh, B.I., Kobayashi, T., Fujisaki, J., Clemens, T.L., Lin, C.P.,
- Kronenberg, H.M., and Scadden, D.T. (2012). Endogenous bone marrow MSCs are
- dynamic, fate-restricted participants in bone maintenance and regeneration. Cell Stem
- 542 Cell *10*, 259-272. 10.1016/j.stem.2012.02.003.

- 543 14. Kim, S., Lee, S., Lim, J., Choi, H., Kang, H., Jeon, N.L., and Son, Y. (2021). Human bone 544 marrow-derived mesenchymal stem cells play a role as a vascular pericyte in the 545 reconstruction of human BBB on the angiogenesis microfluidic chip. Biomaterials *279*, 546 121210. 10.1016/j.biomaterials.2021.121210.
- 547 15. Costa, L.A., Eiro, N., Fraile, M., Gonzalez, L.O., Saá, J., Garcia-Portabella, P., Vega, B., Schneider, J., and Vizoso, F.J. (2021). Functional heterogeneity of mesenchymal stem cells from natural niches to culture conditions: implications for further clinical uses. Cell Mol Life Sci 78, 447-467. 10.1007/s00018-020-03600-0.
- 551 16. Wang, H., Li, D., Zhai, Z., Zhang, X., Huang, W., Chen, X., Huang, L., Liu, H., Sun, J., Zou, Z., et al. (2019). Characterization and Therapeutic Application of Mesenchymal Stem Cells with Neuromesodermal Origin from Human Pluripotent Stem Cells. Theranostics *9*, 1683-1697. 10.7150/thno.30487.
- Ozay, E.I., Vijayaraghavan, J., Gonzalez-Perez, G., Shanthalingam, S., Sherman, H.L.,
 Garrigan, D.T., Jr., Chandiran, K., Torres, J.A., Osborne, B.A., Tew, G.N., et al. (2019).
 Cymerus™ iPSC-MSCs significantly prolong survival in a pre-clinical, humanized mouse
 model of Graft-vs-host disease. Stem Cell Res *35*, 101401. 10.1016/j.scr.2019.101401.
- Wruck, W., Graffmann, N., Spitzhorn, L.-S., and Adjaye, J. (2021). Human Induced Pluripotent Stem Cell-Derived Mesenchymal Stem Cells Acquire Rejuvenation and Reduced Heterogeneity. Front Cell Dev Biol *9*, 717772. 10.3389/fcell.2021.717772.
- 562 19. Zhou, T., Yuan, Z., Weng, J., Pei, D., Du, X., He, C., and Lai, P. (2021). Challenges and advances in clinical applications of mesenchymal stromal cells. J Hematol Oncol *14*, 24. 10.1186/s13045-021-01037-x.
- 565 20. Kim, J.Y., Kim, S.H., Seok, J., Bae, S.H., Hwang, S.-G., and Kim, G.J. (2023). Increased PRL-1 in BM-derived MSCs triggers anaerobic metabolism via mitochondria in a cholestatic rat model. Mol Ther Nucleic Acids *31*, 512-524. 10.1016/j.omtn.2023.01.017.
- 568 21. Johnson, T.V., Bull, N.D., and Martin, K.R. (2009). Transplantation prospects for the inner retina. Eye (Lond) *23*, 1980-1984. 10.1038/eye.2008.376.
- 570 22. Yu, S., Tanabe, T., Dezawa, M., Ishikawa, H., and Yoshimura, N. (2006). Effects of bone 571 marrow stromal cell injection in an experimental glaucoma model. Biochem Biophys Res 572 Commun *344*, 1071-1079.
- 573 23. Dhoke, N.R., Kaushik, K., and Das, A. (2020). Cxcr6-Based Mesenchymal Stem Cell Gene 574 Therapy Potentiates Skin Regeneration in Murine Diabetic Wounds. Mol Ther *28*, 1314-575 1326. 10.1016/j.ymthe.2020.02.014.
- 576 24. Chen, W., Li, M., Cheng, H., Yan, Z., Cao, J., Pan, B., Sang, W., Wu, Q., Zeng, L., Li, Z., et al. (2013). Overexpression of the mesenchymal stem cell Cxcr4 gene in irradiated mice increases the homing capacity of these cells. Cell Biochem Biophys *67*, 1181-1191. 10.1007/s12013-013-9632-6.
- Wynn, R.F., Hart, C.A., Corradi-Perini, C., O'Neill, L., Evans, C.A., Wraith, J.E., Fairbairn, L.J., and Bellantuono, I. (2004). A small proportion of mesenchymal stem cells strongly expresses functionally active CXCR4 receptor capable of promoting migration to bone marrow. Blood *104*, 2643-2645.
- Vallet, S., Pozzi, S., Patel, K., Vaghela, N., Fulciniti, M.T., Veiby, P., Hideshima, T., Santo, L., Cirstea, D., Scadden, D.T., et al. (2011). A novel role for CCL3 (MIP-1α) in myeloma-induced bone disease via osteocalcin downregulation and inhibition of osteoblast

- 587 function. Leukemia *25*, 1174-1181. 10.1038/leu.2011.43.
- 588 27. Muthusamy, A., Lin, C.M., Shanmugam, S., Lindner, H.M., Abcouwer, S.F., and Antonetti,
- D.A. (2014). Ischemia-reperfusion injury induces occludin phosphorylation/ubiquitination
- and retinal vascular permeability in a VEGFR-2-dependent manner. J Cereb Blood Flow
- 591 Metab *34*, 522-531. 10.1038/jcbfm.2013.230.
- 592 28. Liu, L., Jiang, Y., and Steinle, J.J. (2016). Compound 49b Restores Retinal Thickness and
- Reduces Degenerate Capillaries in the Rat Retina following Ischemia/Reperfusion. PLoS
- One *11*, e0159532. 10.1371/journal.pone.0159532.
- 595 29. DeDreu, J., Pal-Ghosh, S., Mattapallil, M.J., Caspi, R.R., Stepp, M.A., and Menko, A.S. (2022).
- 596 Uveitis-mediated immune cell invasion through the extracellular matrix of the lens capsule.
- 597 Faseb j *36*, e21995. 10.1096/fj.202101098R.
- 598 30. Wu, M.Y., Yiang, G.T., Liao, W.T., Tsai, A.P., Cheng, Y.L., Cheng, P.W., Li, C.Y., and Li, C.J.
- 599 (2018). Current Mechanistic Concepts in Ischemia and Reperfusion Injury. Cell Physiol
- Biochem 46, 1650-1667. 10.1159/000489241.
- 601 31. Kalogeris, T., Baines, C.P., Krenz, M., and Korthuis, R.J. (2012). Cell biology of
- ischemia/reperfusion injury. Int Rev Cell Mol Biol 298, 229-317. 10.1016/b978-0-12-
- 603 394309-5.00006-7.
- 32. Zhang, Y., Zhao, L., Wang, X., Ma, W., Lazere, A., Qian, H.H., Zhang, J., Abu-Asab, M., Fariss,
- 605 R.N., Roger, J.E., et al. (2018). Repopulating retinal microglia restore endogenous
- organization and function under CX3CL1-CX3CR1 regulation. Sci Adv 4, eaap8492.
- 607 10.1126/sciadv.aap8492.
- 608 33. Kinuthia, U.M., Wolf, A., and Langmann, T. (2020). Microglia and Inflammatory Responses
- in Diabetic Retinopathy. Front Immunol *11*, 564077. 10.3389/fimmu.2020.564077.
- 610 34. Pesaresi, M., Bonilla-Pons, S.A., Sebastian-Perez, R., Di Vicino, U., Alcoverro-Bertran, M.,
- 611 Michael, R., and Cosma, M.P. (2021). The Chemokine Receptors Ccr5 and Cxcr6 Enhance
- Migration of Mesenchymal Stem Cells into the Degenerating Retina. Mol Ther 29, 804-
- 613 821. 10.1016/j.ymthe.2020.10.026.
- 614 35. Xie, L., Chen, Z., Liu, M., Huang, W., Zou, F., Ma, X., Tao, J., Guo, J., Xia, X., Lyu, F., et al.
- 615 (2020). MSC-Derived Exosomes Protect Vertebral Endplate Chondrocytes against
- Apoptosis and Calcification via the miR-31-5p/ATF6 Axis. Mol Ther Nucleic Acids 22, 601-
- 617 614. 10.1016/j.omtn.2020.09.026.
- 618 36. Yue, R., Lu, S., Luo, Y., Zeng, J., Liang, H., Qin, D., Wang, X., Wang, T., Pu, J., and Hu, H.
- 619 (2022). Mesenchymal stem cell-derived exosomal microRNA-182-5p alleviates
- 620 myocardial ischemia/reperfusion injury by targeting GSDMD in mice. Cell Death Discov 8,
- 621 202. 10.1038/s41420-022-00909-6.
- 622 37. Nakajima, D., Watanabe, Y., Ohsumi, A., Pipkin, M., Chen, M., Mordant, P., Kanou, T., Saito,
- T., Lam, R., Coutinho, R., et al. (2019). Mesenchymal stromal cell therapy during ex vivo
- lung perfusion ameliorates ischemia-reperfusion injury in lung transplantation. J Heart
- 625 Lung Transplant *38*, 1214-1223. 10.1016/j.healun.2019.07.006.
- 626 38. Cao, H., Cheng, Y., Gao, H., Zhuang, J., Zhang, W., Bian, Q., Wang, F., Du, Y., Li, Z., Kong,
- D., et al. (2020). In Vivo Tracking of Mesenchymal Stem Cell-Derived Extracellular Vesicles
- Improving Mitochondrial Function in Renal Ischemia-Reperfusion Injury. ACS Nano 14,
- 629 4014-4026. 10.1021/acsnano.9b08207.
- 630 39. Qiu, L., Cai, Y., Geng, Y., Yao, X., Wang, L., Cao, H., Zhang, X., Wu, Q., Kong, D., Ding, D.,

- et al. (2022). Mesenchymal stem cell-derived extracellular vesicles attenuate tPA-induced
- blood-brain barrier disruption in murine ischemic stroke models. Acta Biomater *154*, 424-
- 633 442. 10.1016/j.actbio.2022.10.022.
- 634 40. Kim, J.H., Kim, J.H., Park, J.A., Lee, S.-W., Kim, W.J., Yu, Y.S., and Kim, K.-W. (2006). Blood-
- 635 neural barrier: intercellular communication at glio-vascular interface. J Biochem Mol Biol 39, 339-345.
- 41. Zhao, Z., Nelson, A.R., Betsholtz, C., and Zlokovic, B.V. (2015). Establishment and Dysfunction of the Blood-Brain Barrier. Cell *163*, 1064-1078. 10.1016/j.cell.2015.10.067.
- 42. Mölzer, C., Heissigerova, J., Wilson, H.M., Kuffova, L., and Forrester, J.V. (2020). Immune
- Privilege: The Microbiome and Uveitis. Front Immunol *11*, 608377.
- 641 10.3389/fimmu.2020.608377.
- 642 43. Spadoni, I., Fornasa, G., and Rescigno, M. (2017). Organ-specific protection mediated by
- cooperation between vascular and epithelial barriers. Nat Rev Immunol *17*, 761-773.
- 644 10.1038/nri.2017.100.
- 645 44. Bosma, E.K., van Noorden, C.J.F., Schlingemann, R.O., and Klaassen, I. (2018). The role of
- plasmalemma vesicle-associated protein in pathological breakdown of blood-brain and
- blood-retinal barriers: potential novel therapeutic target for cerebral edema and diabetic
- 648 macular edema. Fluids Barriers CNS 15, 24. 10.1186/s12987-018-0109-2.
- 649 45. Galipeau, J., and Sensébé, L. (2018). Mesenchymal Stromal Cells: Clinical Challenges and Therapeutic Opportunities. Cell Stem Cell *22*, 824-833. 10.1016/j.stem.2018.05.004.
- 651 46. Lou, Y.-L., Guo, F., Liu, F., Gao, F.-L., Zhang, P.-Q., Niu, X., Guo, S.-C., Yin, J.-H., Wang, Y.,
- and Deng, Z.-F. (2012). miR-210 activates notch signaling pathway in angiogenesis
- 653 induced by cerebral ischemia. Mol Cell Biochem *370*, 45-51. 10.1007/s11010-012-1396-654 6.
- 47. Jean LeBlanc, N., Guruswamy, R., and ElAli, A. (2018). Vascular Endothelial Growth Factor
- 656 Isoform-B Stimulates Neurovascular Repair After Ischemic Stroke by Promoting the
- Function of Pericytes via Vascular Endothelial Growth Factor Receptor-1. Mol Neurobiol
- 658 55, 3611-3626. 10.1007/s12035-017-0478-6.
- 48. Park, H.J., Shin, J.Y., Kim, H.N., Oh, S.H., Song, S.K., and Lee, P.H. (2015). Mesenchymal
- stem cells stabilize the blood-brain barrier through regulation of astrocytes. Stem Cell Res
- 661 Ther 6, 187. 10.1186/s13287-015-0180-4.
- 662 49. Tamaki, M., Kidoguchi, K., Mizobe, T., Koyama, J., Kondoh, T., Sakurai, T., Kohmura, E.,
- Yokono, K., and Umetani, K. (2006). Carotid artery occlusion and collateral circulation in
- 664 C57Black/6J mice detected by synchrotron radiation microangiography. Kobe J Med Sci
- 665 *52*, 111-118.
- 666 50. Li, W., Huang, L., Zeng, J., Lin, W., Li, K., Sun, J., Huang, W., Chen, J., Wang, G., Ke, Q., et al.
- 667 (2018). Characterization and transplantation of enteric neural crest cells from human
- 668 induced pluripotent stem cells. Mol Psychiatry 23, 499-508. 10.1038/mp.2016.191.
- 51. Li, L., Du, G., Wang, D., Zhou, J., Jiang, G., and Jiang, H. (2017). Overexpression of Heme
- 670 Oxygenase-1 in Mesenchymal Stem Cells Augments Their Protection on Retinal Cells In
- Vitro and Attenuates Retinal Ischemia/Reperfusion Injury In Vivo against Oxidative Stress.
- 672 Stem Cells Int *2017*, 4985323. 10.1155/2017/4985323.
- 673 52. Morikawa, S., Mabuchi, Y., Kubota, Y., Nagai, Y., Niibe, K., Hiratsu, E., Suzuki, S., Miyauchi-
- Hara, C., Nagoshi, N., Sunabori, T., et al. (2009). Prospective identification, isolation, and

- systemic transplantation of multipotent mesenchymal stem cells in murine bone marrow.

 J Exp Med *206*, 2483-2496. 10.1084/jem.20091046.
- 53. Jiang, D., Xiong, G., Feng, H., Zhang, Z., Chen, P., Yan, B., Chen, L., Gandhervin, K., Ma, C., Li, C., et al. (2019). Donation of mitochondria by iPSC-derived mesenchymal stem cells protects retinal ganglion cells against mitochondrial complex I defect-induced degeneration. Theranostics *9*, 2395-2410. 10.7150/thno.29422.
- 54. Liu, J., Li, W., Wang, Y., Fan, W., Li, P., Lin, W., Yang, D., Fang, R., Feng, M., Hu, C., et al. (2014). Islet-1 overexpression in human mesenchymal stem cells promotes vascularization through monocyte chemoattractant protein-3. Stem Cells 32, 1843-1854. 10.1002/stem.1682.

FIGURE LEGENDS

Fig. 1 BRB breakdown after retinal I/R

Fig. 2 CCL5 expression increased and colocalized with the BRB after retinal I/R

(A) KEGG pathway enrichment analysis was performed for retinas from the sham and 702 1 d after retinal I/R groups to explore the possible signaling pathways that changed after 703 retinal I/R (n=3 mice per group). (B) qPCR was performed to measure the expression 704 of CCL2, CCL5, CCL7, CCL12, CXCL2, and CXCL12 in retinas from the sham and 1 705 706 d after retinal I/R groups (n=6 mice per group). (C) qPCR was performed to compare the expression of CCL5 in retinas from the sham, 6 h, 1 d and 3 d after retinal I/R groups 707 (n=6 mice per group). (D-E) Flow cytometry analysis and quantification of the MFI of 708 CCL5 in retinas from the sham and 1 d after retinal I/R groups (n=4 mice per group). 709 (F) Representative confocal fluorescence images of the distribution of CCL5 (red) 710 around IB4⁺ blood vessels (green) in retinas from the sham and 1 d after retinal I/R 711 groups. Scale bar, 50 µm. (G) Scheme (left) of the structure of the retina and the division 712 of the retinal plexus into three layers, namely, the superficial, intermediate and deep 713 layers. Quantification (right) of the percentage of vessels colocalized with CCL5 in 714 each layer. Analysis and statistics of colocalization were performed via ImageJ and a 715 plug-in named coloc2. The data are expressed as the mean \pm SEM. All statistical 716 significance was calculated using Student's t test or two-way ANOVA. *p <0.05; **p 717 <0.01; ****p <0.0001; ns, not significant. 718

719

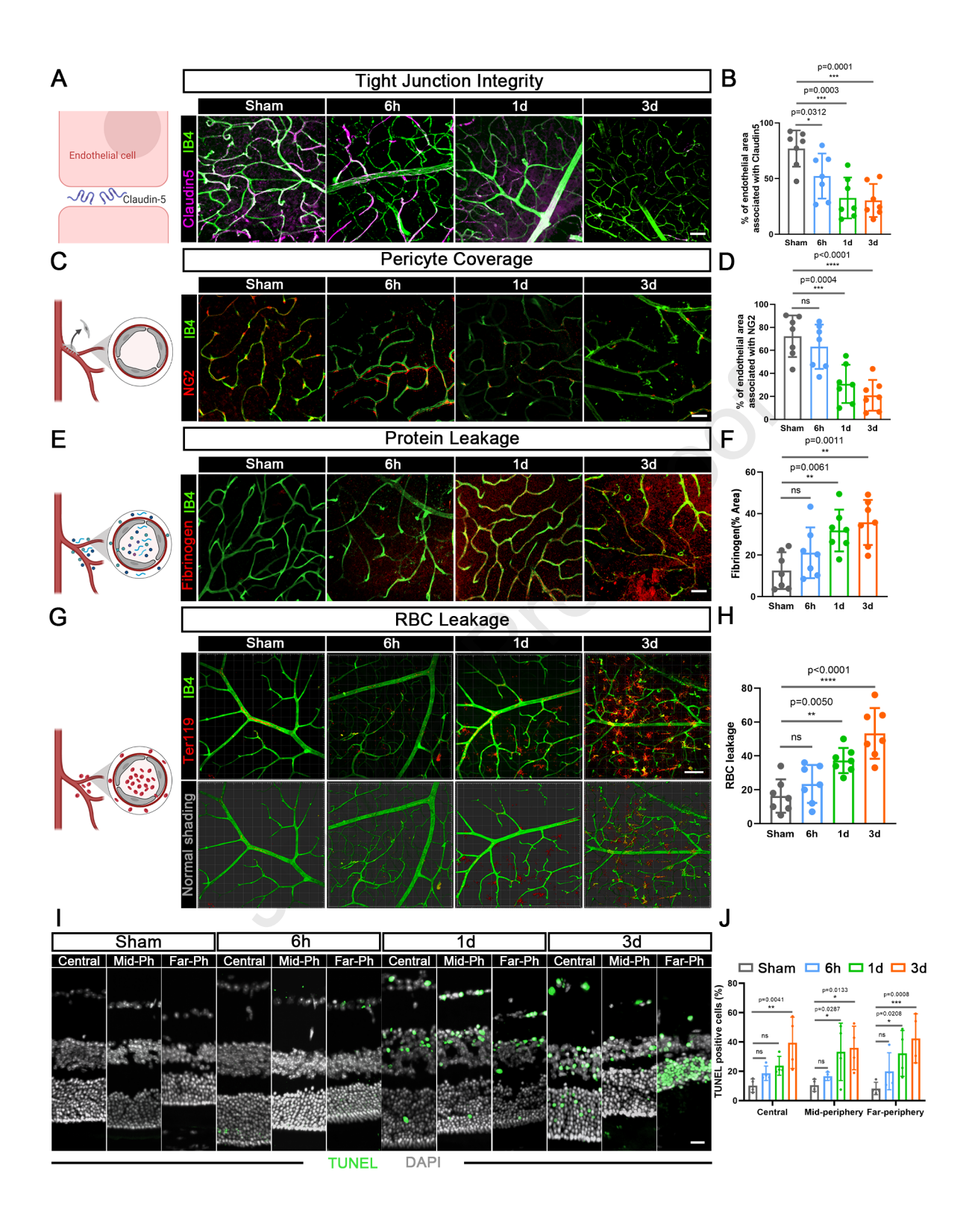
- Fig. 3 Overexpression of CCR5 improved the migratory capacity of iMSCs in vitro
- and the vascular colonization capacity of iMSCs in vivo
- 722 (A) Transwell migration assays were performed to compare the migratory capacity of
- 723 iMSC^{tdTomato} and iMSC^{CCR5} under the recruitment of hCCL5 and mCCL5 respectively.

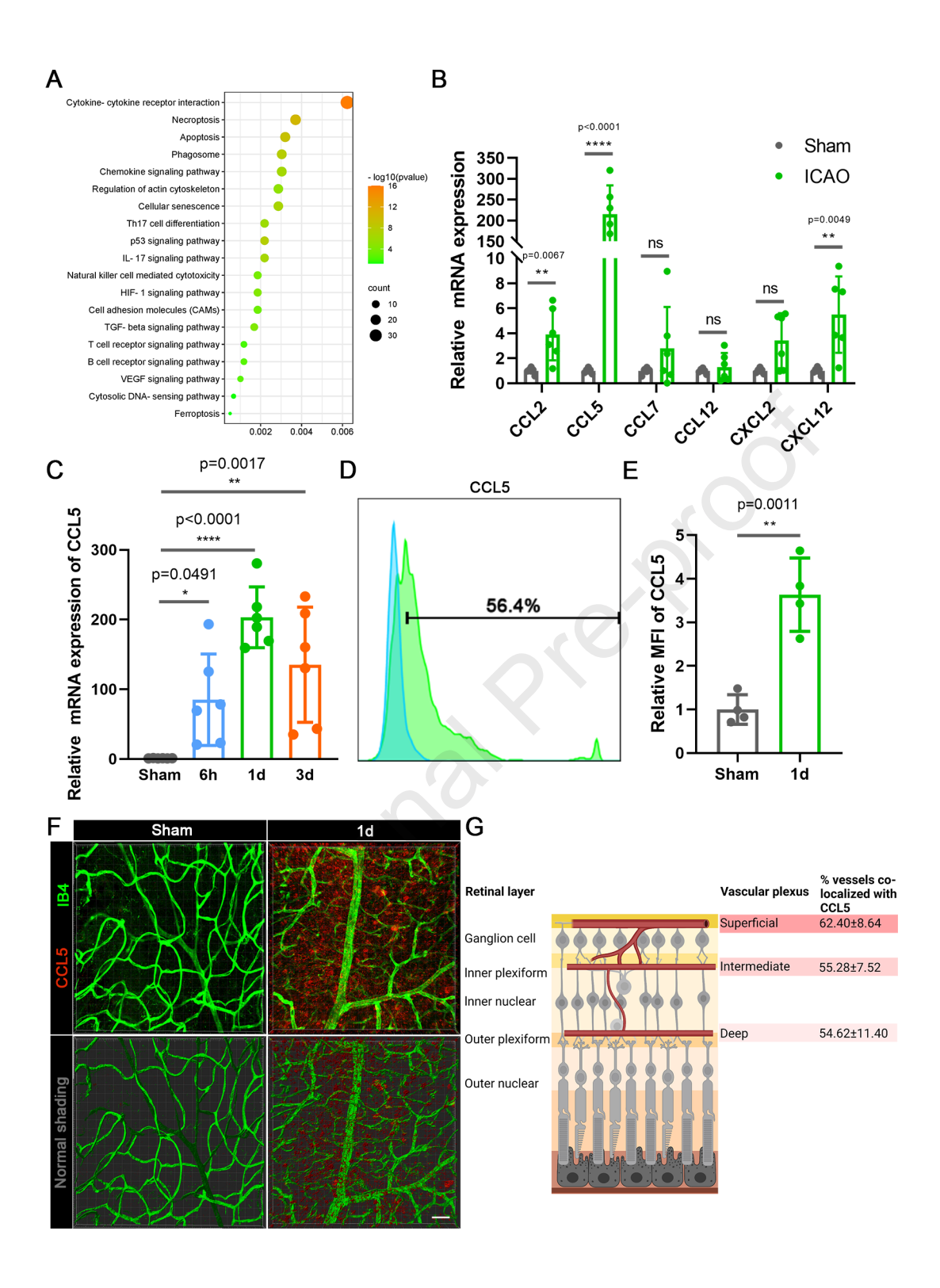
Scale bars, 100 μ m. (B) Pattern (upward) and quantification of the transwell migration assay results. (C) Representative images of iMSC^{CCR5} (red) and iMSC^{tdTomato} (red) retained in retinas at 4 dpt and 7 dpt from the sham and retinal I/R groups. Scale bar, 100 μ m. (D) Pattern (upward) and quantification analyses of the number of iMSC^{CCR5} and iMSC^{tdTomato} retained in retinas and their percentages on vessels at 4 dpt and 7 dpt in the sham and retinal I/R groups (n=6 mice per group). The data are expressed as the mean \pm SEM. All statistical significance was calculated using one- or two-way ANOVA. **p <0.01; ***p <0.001; ns, not significant.

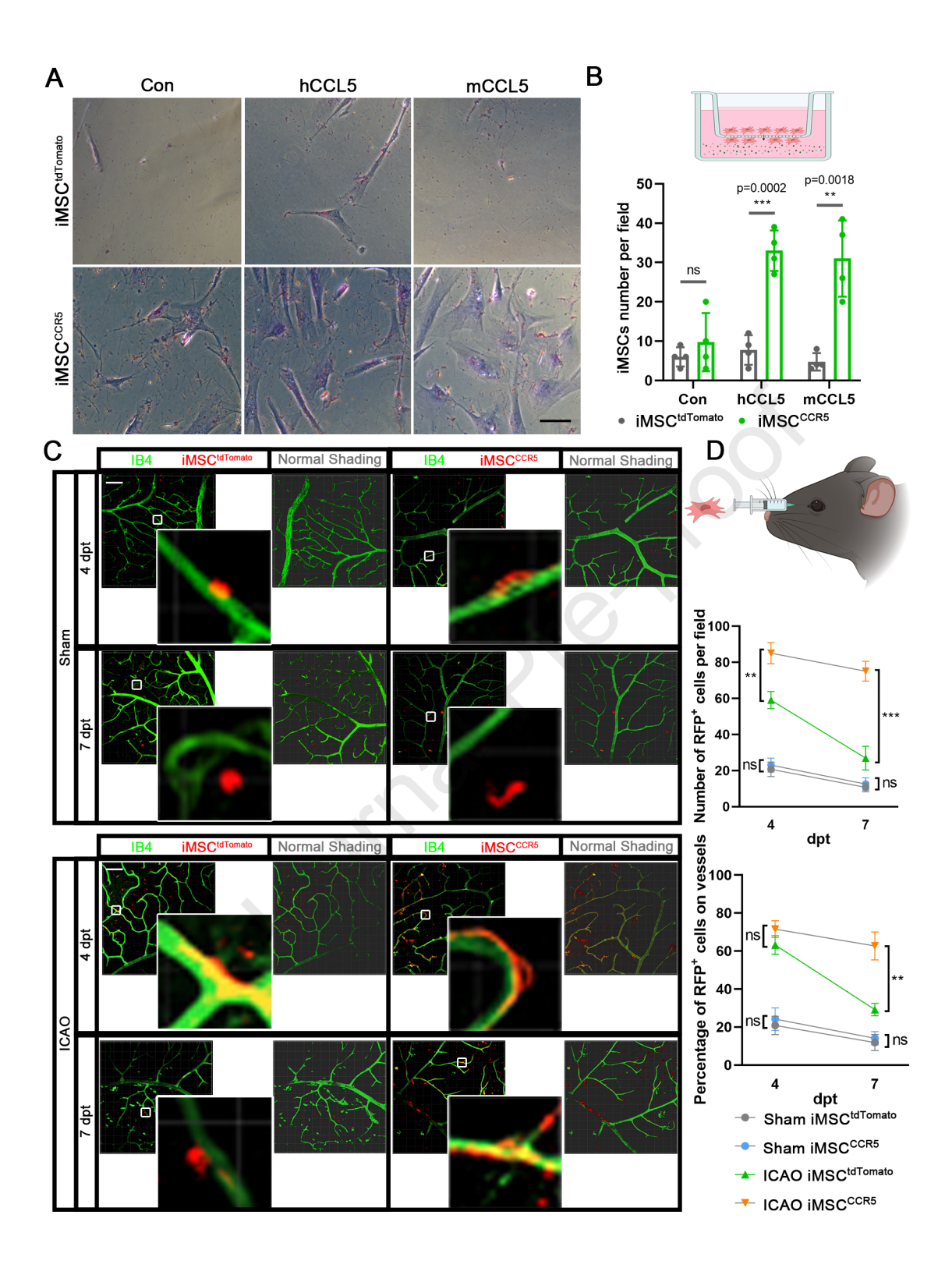
Fig. 4 iMSC^{CCR5} infusion reversed damage to the BRB caused by retinal I/R

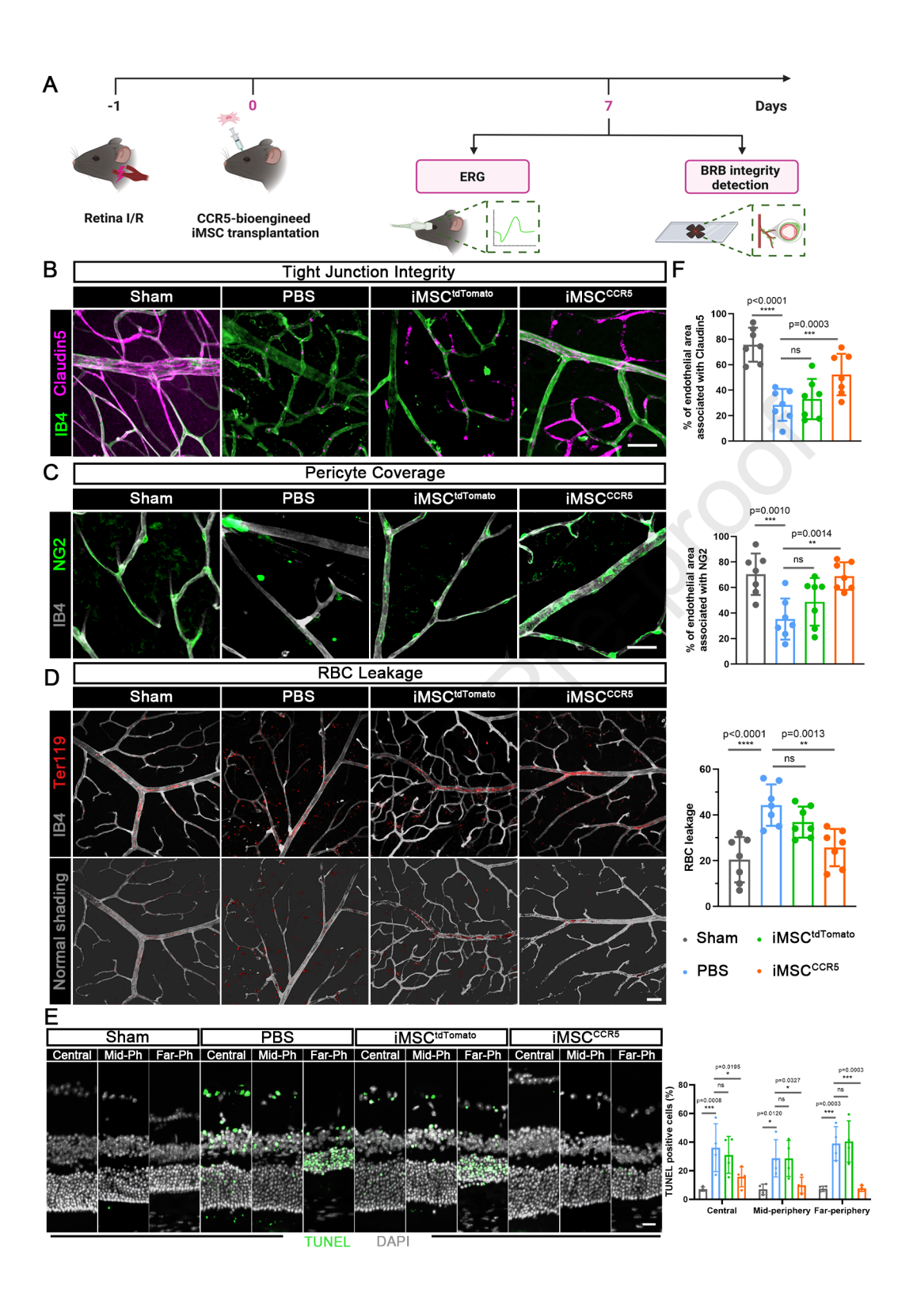
(A) Scheme of the evaluation of iMSC-based therapy on retinal I/R. (B-D, F) Representative confocal fluorescence images and quantification of the distribution of Claudin5 (purple) associated with IB4⁺ blood vessels (green), NG2⁺ pericyte (green) coverage of IB4⁺ blood vessels (gray), and Ter119⁺ RBCs (red) leakage in retinas from the sham, PBS, iMSC^{tdTomato} and iMSC^{CCR5} groups (n=7 mice per group). Scale bar, 50 μ m. (E) Representative confocal fluorescence images of TUNEL staining and quantification of TUNEL-positive rates in the Central, Mid-Ph and Far-Ph positions of retinas from the sham, PBS, iMSC^{tdTomato} and iMSC^{CCR5} groups (n=4 mice per group). Scale bar, 20 μ m. The data are expressed as the mean \pm SEM. All statistical significance was calculated using one- or two-way ANOVA. *p <0.05; **p <0.01; ***p <0.001; ns, not significant.

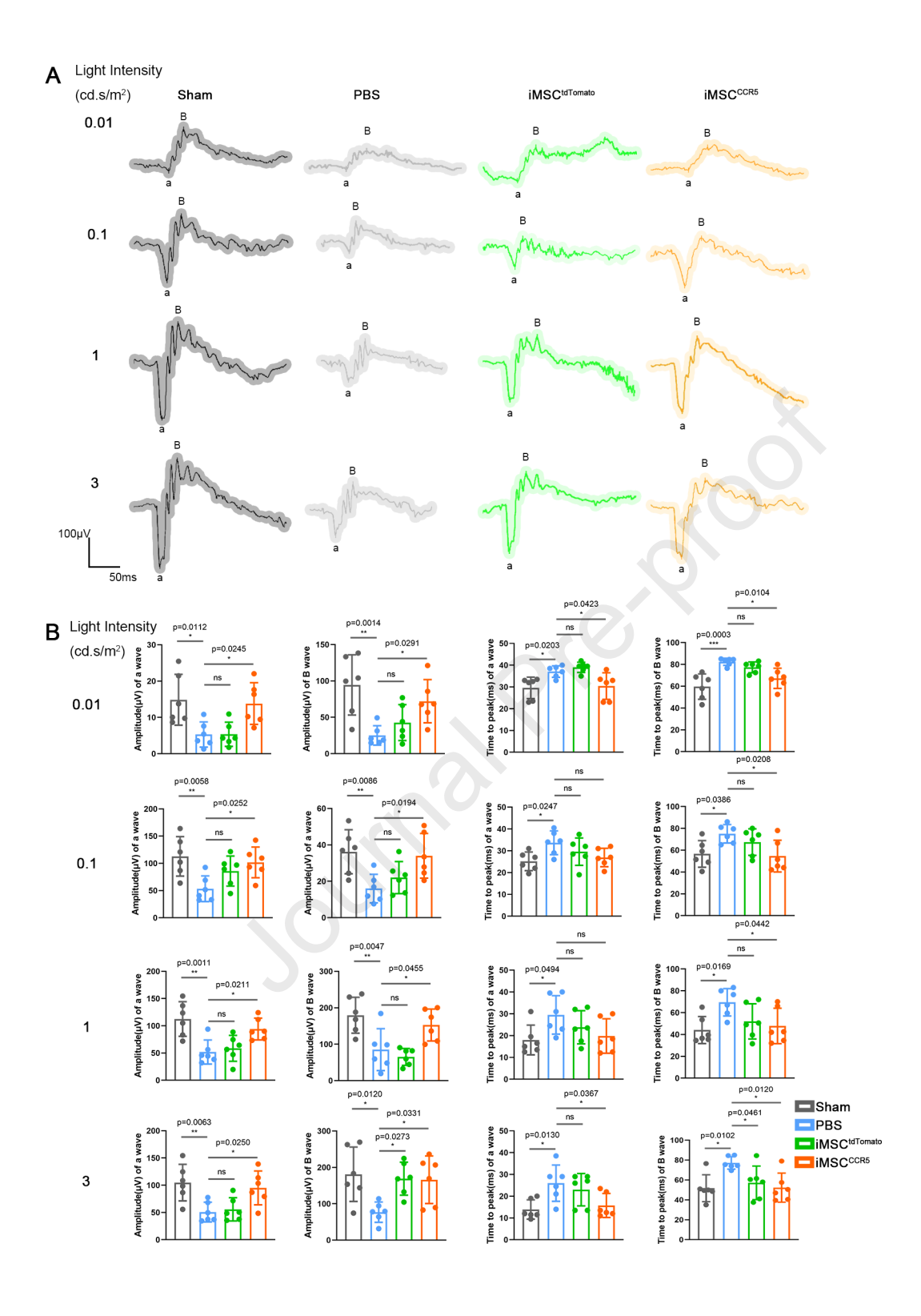
746	Fig. 5 iMSC ^{CCR5} infusion recovered damage to visual function caused by retinal
747	I/R
748	(A, B) ERG of amplitude and the time to peak of a- and b-waves among the sham, PBS,
749	iMSC ^{tdTomato} and iMSC ^{CCR5} groups (n=6 mice per group). The light intensity consisted
750	of 4 increasing levels (dim to bright), including 0.01, 0.1, 1 and 3 cd.s/m ² . The data are
751	expressed as the mean \pm SEM. All statistical significance was calculated using one-way
752	ANOVA. * $p < 0.05$; ** $p < 0.01$; *** $p < 0.001$; ns, not significant.
753	











Tao Li and colleagues conducted this study to offer new insights into genetically modulated mesenchymal stromal cells acting as biopatches to restore blood-retinal barrier integrity for treating vision-threatening retinal diseases associated with retinal ischemia/reperfusion.